Phenotype of ribonuclease 1 deficiency in mice

EMILY R. GARNETT,[1,2] JO E. LOMAX,[3] BASSEM M. MOHAMMED,[4] DAVID GAILANI,[4] JOHN P. SHEEHAN,[5] and RONALD T. RAINES[2,6,7]

[1]Graduate Program in Molecular and Cellular Pharmacology, University of Wisconsin–Madison, Madison, Wisconsin 53706, USA
[2]Department of Chemistry, Massachusetts Institute of Technology, Cambridge, Massachusetts 02139, USA
[3]Graduate Program Molecular and Cellular and Molecular Biology, University of Wisconsin–Madison, Madison, Wisconsin 53706, USA
[4]Department of Pathology, Microbiology and Immunology, Vanderbilt University Medical Center, Nashville, Tennessee 37232, USA
[5]Department of Medicine/Hematology–Oncology, University of Wisconsin–Madison, Madison, Wisconsin 53706, USA
[6]Department of Biochemistry, University of Wisconsin–Madison, Madison, Wisconsin 53706, USA
[7]Department of Chemistry, University of Wisconsin–Madison, Madison, Wisconsin 53706, USA

ABSTRACT

Biological roles for extracellular RNA (eRNA) have become apparent. For example, eRNA can induce contact activation in blood via activation of the plasma proteases factor XII (FXII) and factor XI (FXI). We sought to reveal the biological role of the secretory enzyme ribonuclease 1 (RNase 1) in an organismal context by generating and analyzing RNase 1 knockout (*Rnase1*$^{-/-}$) mice. We found that these mice are viable, healthy, and fertile, though larger than *Rnase1*$^{+/+}$ mice. *Rnase1*$^{-/-}$ plasma contains more RNA than does the plasma of *Rnase1*$^{+/+}$ mice. Moreover, the plasma of *Rnase1*$^{-/-}$ mice clots more rapidly than does wild-type plasma. This phenotype appeared to be due to increased levels of the active form of FXII (FXIIa) in the plasma of *Rnase1*$^{-/-}$ mice compared to *Rnase1*$^{+/+}$ mice, and is consistent with the known effects of eRNA on FXII activation. The apparent activity of FXI in the plasma of *Rnase1*$^{-/-}$ mice was 1000-fold higher when measured in an assay triggered by a low concentration of tissue factor than in assays based on recalcification, consistent with eRNA enhancing FXI activation by thrombin. These findings suggest that one of the physiological functions of RNase 1 is to degrade eRNA in blood plasma. Loss of this function facilitates FXII and FXI activation, which could have effects on inflammation and blood coagulation. We anticipate that *Rnase1*$^{-/-}$ mice will be a useful tool for evaluating other hypotheses about the functions of RNase 1 and of eRNA in vivo.

Keywords: blood coagulation; eRNA; gene knockout; mouse; ribonuclease

INTRODUCTION

Ribonuclease 1 (RNase 1) is a vertebrate secretory protein with robust nonspecific ribonucleolytic activity. The physical and catalytic properties of this enzyme are well understood due to its similarity to RNase A, a bovine homolog of RNase 1 that served as a model protein for seminal studies in biological chemistry during the twentieth century (D'Alessio and Riordan 1997; Raines 1998; Marshall et al. 2008; Cuchillo et al. 2011). RNase 1 is a member of a large superfamily termed the pancreatic-type ribonucleases (ptRNases) or vertebrate secretory ribonucleases. ptRNases play diverse biological roles (Sorrentino 2010; Koczera et al. 2016; Lu et al. 2018) and might have evolved convergently in bacteria (Cuthbert et al. 2018).

No specific biological function has been identified for RNase 1. Early hypotheses focused on digestion, as RNase A is abundant in the pancreas of ruminants (Barnard 1969). This hypothesis is challenged by recent work demonstrating nondigestive activities when human RNase 1 variants and conjugates are administered exogenously in vitro and in vivo (Strong et al. 2012; D'Avino et al. 2016; Hoang et al. 2018).

RNase 1 has the highest catalytic activity and the widest expression pattern of the ptRNases, and is found in many bodily fluids (Morita et al. 1986; Su et al. 2004). In humans and mice, RNase 1 circulates in blood plasma at ~0.5 μg/mL (Weickmann et al. 1984). The major source of plasma RNase 1 is the vascular endothelium (Landré et al. 2002; Fischer et al. 2011), and the pH optimum for its enzymatic activity (7.3) is close to the pH of blood (Eller et al. 2014). These findings suggest that RNase 1 could be active within the vasculature.

Corresponding author: rtraines@mit.edu
Article is online at http://www.rnajournal.org/cgi/doi/10.1261/rna.070433.119.

Recent studies have highlighted the ability of RNase A to exert biological effects via degradation of extracellular RNA (eRNA), which is known to play roles in immunity and blood coagulation, as well as in cancer and artherosclerosis (Kannemeier et al. 2007; Fischer et al. 2012, 2013; Simsekyilmaz et al. 2014). RNA enhances reciprocal activation of the blood plasma proteins factors XII (FXII) and prekallikrein to the active protease forms FXIIa and kallikrein by a process called contact activation that requires physical interaction between RNA and the enzymes (Kannemeier et al. 2007). Both FXIIa and kallikrein catalyze reactions that are proinflammatory. RNA also enhances activation of the plasma coagulation protease FXI by both FXIIa and thrombin, promoting blood clotting (Gajsiewicz et al. 2017). The importance of these reactions in vivo is suggested by the observations that RNase A produces a beneficial anticoagulant effect in murine models of arterial thrombosis (Kannemeier et al. 2007) and stroke (Walberer et al. 2009), and that RNase 1 is cardioprotective in humans (Cabrera-Fuentes et al. 2015). Here, we report on the first generation of an *Rnase1* knockout (KO) mouse and the characterization of its phenotype, focusing on plasma RNA and blood coagulation.

RESULTS

Generation of *Rnase1*$^{-/-}$ mice by Cre–LoxP recombination

Prior to generating *Rnase1*$^{-/-}$ mice, we sought to validate the use of murine RNase 1 as a model for the human enzyme. Previously, we showed that the murine RI·RNase 1 complex is highly similar to its human homolog in its three-dimensional structure (Lomax et al. 2014). Further, murine RNase 1 exhibits ribonucleolytic activity similar to that of the human enzyme (Lomax et al. 2017). Given that human *Rnase1* is expressed ubiquitously (Futami et al. 1997), we analyzed 18 mouse tissues for *Rnase1* expression by qPCR and found the mRNA to be expressed ubiquitously (Fig. 1A). The in vitro structure–function data, coupled with a similarly broad expression pattern in vivo, instilled confidence in murine RNase 1 as a model for human RNase 1.

Given the unknown biological function of RNase 1, we chose a conditional KO approach to generate mice lacking *Rnase1* expression. The entire *Rnase1* protein-coding exon was flanked with *loxP* sites in the gene-targeting vector, allowing Cre-mediated recombination to excise this exon

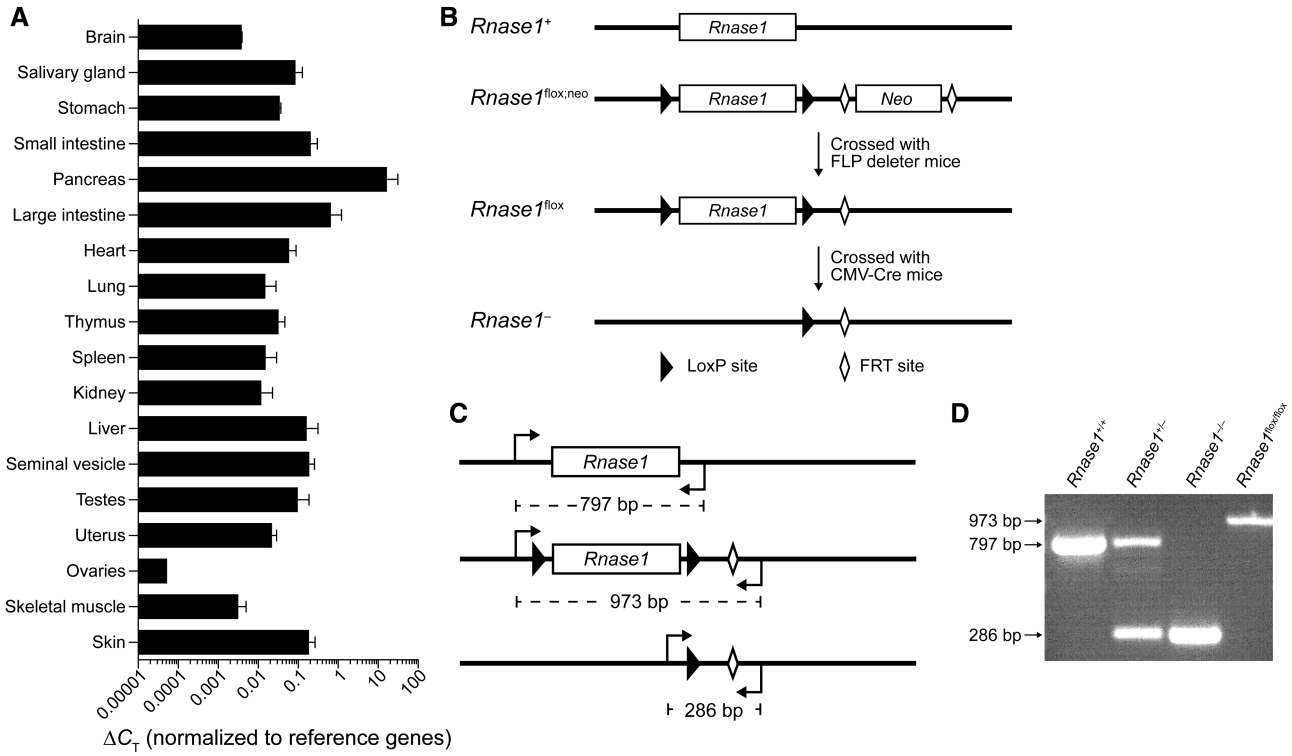

FIGURE 1. Generation of *Rnase1* KO mice. (*A*) Bar graph showing the tissue-specific expression of *Rnase1* in wild-type mice as measured by qPCR. Data were normalized to the geometric mean of three reference genes. $n = 3$ per tissue. (*B*) Scheme showing the breeding strategy used to generate conditional *Rnase1* KO mice. *Rnase1* refers to the single coding exon for the *Rnase1* gene; *Neo* refers to a neomycin-resistance cassette. (*C*) Scheme showing the genotyping strategy used to identify *Rnase1* alleles. One pair of primers recognizes sites 3′ and 5′ to the targeted exon, enabling identification of wild-type (*top*), targeted/floxed (*center*), and KO (*bottom*) individuals. As in panel *B*, black triangles represent loxP sites, and open diamonds represent FRT sites. (*D*) A representative genotyping gel, showing bands indicative of wild-type, heterozygous, and *Rnase1*$^{-/-}$ mice, as well as *Rnase1*$^{flox/flox}$ mice.

and result in an ablation of *Rnase1* expression. Disruption of the *Rnase1* gene was verified by a Southern blot (Supplemental Fig. S1).

Rnase1$^{-/-}$ mice express neither *Rnase1* mRNA nor RNase 1 protein

qPCR was performed to verify loss of *Rnase1* expression in *Rnase1*$^{-/-}$ mice. Eighteen tissue types were tested for *Rnase1* expression in *Rnase1*$^{-/-}$ and *Rnase1*$^{+/+}$ mice, and levels were normalized to three reference genes. Samples from *Rnase1*$^{-/-}$ mice exhibited virtually undetectable *Rnase1* expression (average $C_T = 34 \pm 0.3$ cycles in samples with amplification) (Fig. 2A). Any nonzero values are likely due to cross-reactivity of the qPCR primers with mRNA of RNase 1 homologs.

We performed zymogram assays of plasma samples to detect RNase 1 by its ribonucleolytic activity and by its electrophoretic mobility. Ribonucleolytic activity as determined by the intensity of all bands on the zymogram was reduced significantly in *Rnase1*$^{-/-}$ samples relative to *Rnase1*$^{+/+}$ samples, representing a 69 ± 6% loss of ribonucleolytic activity (Fig. 2B). A comparable reduction was apparent in solution-phase assays of ribonucleolytic activity in plasma samples, with an estimated total ribonuclease loss of 52 ± 5% in males and 47 ± 2% in females (Fig. 2C).

We hypothesized that residual ribonucleolytic activity in *Rnase1*$^{-/-}$ plasma is due to other ptRNases. Members of this superfamily migrate at distinct rates during SDS–PAGE due to variation in molecular mass and charge. Given that RNase 1 and other ptRNases can be glycosylated in vivo (Beintema et al. 1984; Salazar et al. 2014; Ressler and Raines 2019), we treated plasma samples with PNGase F to reduce sample complexity, and measured mobility of the major ensuing band relative to an aglycosylated recombinant murine RNase 1 standard produced in *E. coli*. We found that whereas *Rnase1*$^{+/+}$ plasma produced a band with mobility 101.2 ± 0.5% that of the RNase 1 standard, *Rnase1*$^{-/-}$ plasma does not, with the closest mobility being 103.5 ± 0.5% that of the standard (Fig. 2D). These results indicate that RNase 1 production was lost in *Rnase1*$^{-/-}$ mice, and confirm that residual ribonucleolytic activity in these mice arises from the activity of other ribonucleases. qPCR analysis of secretory ribonuclease genes in *Rnase1*$^{+/+}$ and *Rnase1*$^{-/-}$ showed the up-regulation of transcripts upon loss of *Rnase1*, notably those of *Rnase4* and *Ang1* (Fig. 3). qPCR analysis of *Rnh1* mRNA showed less variation, except in skeletal muscle (Fig. 3).

Rnase1$^{-/-}$ mice are viable and appear physically normal

Genotyping of initial *Rnase1*$^{flox/flox}$ × B6.C-Tg(CMV–cre) 1Cgn/J progeny revealed that *Rnase1*$^{-/-}$ mice are viable. In heterozygote crosses, the *Rnase1*$^{-}$ allele was inherited according to expected Mendelian ratios, χ^2 (2, $n = 243$) = 9.62, $P < 0.05$. *Rnase1*$^{-/-}$ males and females are both fertile, with crosses of *Rnase1*$^{-/-}$ mice producing litters of identical size and sex distribution (7.4 ± 1 pups per litter, 39 ± 9% male, $n = 67$) to *Rnase1*$^{+/+}$ mice (7.8 ± 2 pups per litter, 39 ± 11% male, $n = 39$).

Rnase1$^{-/-}$ mice of both sexes are significantly heavier than are *Rnase1*$^{+/+}$ mice (Fig. 4A,B), but do not exhibit any other obvious physical phenotype. Gross necropsy and histopathological analyses did not reveal differences between *Rnase1*$^{-/-}$ and *Rnase1*$^{+/+}$ littermates (data not shown). *Rnase1*$^{-/-}$ also exhibit similar longevity to *Rnase1*$^{+/+}$ mice, with a median survival time of 102 wk versus 126 wk (Fig. 4C).

Loss of *Rnase1* results in increased plasma RNA

Given the reduced plasma ribonucleolytic activity in mice lacking *Rnase1* (Fig. 2B–D), we anticipated elevated plasma RNA concentrations in *Rnase1*$^{-/-}$ mice. RNA was isolated from plasma and quantified by spectrophotometry and with a Bioanalyzer electrophoresis system. Whereas their plasma RNA does not appear to differ in size (Supplemental Fig. S2), *Rnase1*$^{-/-}$ mice have significantly elevated levels of RNA in their plasma compared to *Rnase1*$^{+/+}$ mice (Fig. 4D, E). The slightly higher level of RNA observed by spectrophotometry (Fig. 4D) is likely due to the Bioanalyzer only detecting RNA strands that contain >6 nt (Fig. 4E).

Rnase1$^{-/-}$ plasma clots more quickly than does *Rnase1*$^{+/+}$ plasma

Extracellular RNA can stimulate plasma coagulation in vitro through activation of the contact system (Kannemeier et al. 2007). To evaluate whether increased endogenous RNA in *Rnase1*$^{-/-}$ mice results in enhanced plasma coagulation, we carried out a series of kinetic coagulation studies.

Plasma collected into sodium citrate from *Rnase1*$^{-/-}$ mice formed fibrin clots significantly more quickly after recalcification than did plasma from *Rnase1*$^{+/+}$ mice. The respective values were 7.2 ± 1.0 min and 10.6 ± 2.0 min for males, and 5.9 ± 0.8 min and 23.9 ± 6.2 min for females (Fig. 5A,B). Induction of coagulation via the intrinsic pathway with Actin FSL activated partial thromboplastin time (aPTT) reagent reduced clotting time relative to unstimulated plasma, but did not reveal significant differences between clotting in plasma from *Rnase1*$^{-/-}$ and *Rnase1*$^{+/+}$ mice. This distinction is expected, as the aPTT reagent contains a charged substance that will substitute for RNA as an inducer of contact activation.

Inducing coagulation through the extrinsic pathway by addition of a tissue factor–containing reagent (Thromborel S) also resulted in significantly shorter clotting times in *Rnase1*$^{-/-}$ samples relative to *Rnase1*$^{+/+}$ in female mice.

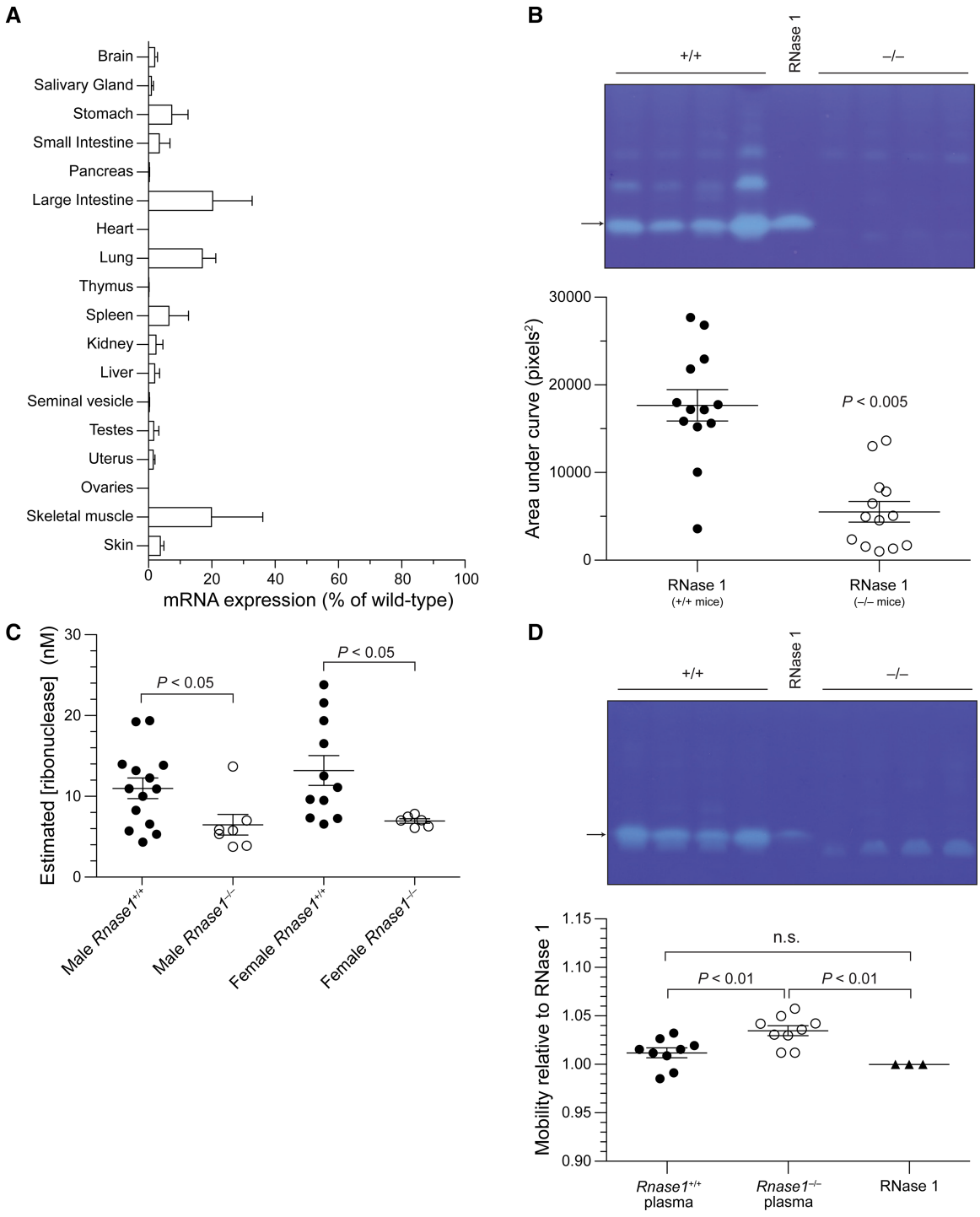

FIGURE 2. Verification of the loss of RNase 1 in *Rnase1*$^{-/-}$ mice. (*A*) Bar graph showing the tissue-specific expression of *Rnase1* in *Rnase1*$^{-/-}$ mice relative to that in *Rnase1*$^{+/+}$ littermates as measured by qPCR. Mice were matched for sex. $n = 3$ per tissue. Data were normalized to the geometric mean of three reference genes. (*B*) Zymogram of plasma samples (0.5 µL) from *Rnase1*$^{+/+}$ or *Rnase1*$^{-/-}$ mice used to evaluate ribonucleolytic activity relative to recombinant murine RNase 1 (100 pmol; arrow). Graph showing total ribonucleolytic activity, which was quantified by integration of a densitometry map of each lane and found to be significantly lower in *Rnase1*$^{-/-}$ mice than in *Rnase1*$^{+/+}$ mice. (*C*) Graph showing plasma ribonuclease concentration by genotype and sex as estimated from ribonucleolytic activity. Concentration was calculated with Equation 1 and $k_{cat}/K_M = 8.6 \times 10^6$ M^{-1} sec^{-1}. $n \geq 6$. (*D*) Zymogram of plasma samples (0.5 µL) treated with PNGase F and of recombinant murine RNase 1 (100 pmol; arrow). The mobility was measured from the position of the well, and normalized to the mobility of recombinant murine RNase 1 (*center* lane). The position of the primary band present in *Rnase1*$^{-/-}$ plasma differs from that in wild-type plasma (arrow).

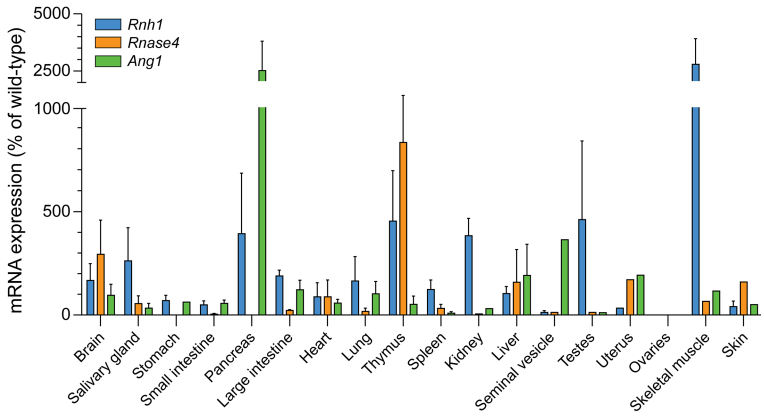

FIGURE 3. Bar graph showing the tissue-specific expression of relevant genes in *Rnase1*$^{-/-}$ mice relative to that in *Rnase1*$^{+/+}$ littermates as measured by qPCR. *Rnh1* encodes ribonuclease inhibitor, *Rnase4* encodes RNase 4, and *Ang1* encodes angiogenin 1. Mice were matched for sex. $n = 3$. Data were normalized to *Gapdh*.

This effect was detectable at a high (saturating) concentration of tissue factor (3.52 ± 0.40 min for *Rnase1*$^{-/-}$ vs. 5.26 ± 0.28 min for *Rnase1*$^{+/+}$) but was more pronounced at a limiting concentration of tissue factor (5.81 ± 0.83 min for *Rnase1*$^{-/-}$ vs. 12.9 ± 3.5 min for *Rnase1*$^{+/+}$).

Additional experiments were performed to investigate potential causes for the differences in coagulation times unrelated to contact activation and the intrinsic pathway. Tissue factor expression is elevated in obesity (Samad and Ruf 2013), and *Rnase1*$^{-/-}$ mice are heavier than *Rnase1*$^{+/+}$ mice. Tissue factor expression was, however, similar in *Rnase1*$^{-/-}$ and *Rnase1*$^{+/+}$ mice (Fig. 5C). Fibrinogen levels, as measured by ELISA, were likewise similar in the two mouse lines (Fig. 5D).

Apparent FXII and FXI activity are elevated in plasma from *Rnase1*$^{-/-}$ mice

Coagulation induced with Actin FSL aPTT reagent was similar in *Rnase1*$^{+/+}$ and *Rnase1*$^{-/-}$ mice (Fig. 6A), indicating that the intrinsic pathway of coagulation is intact in both lines. The specific activity of FXII appeared, however, to be increased by two- to threefold in *Rnase1*$^{-/-}$ mice when clotting was induced without an activator, and more than 100-fold in the presence of Actin FSL, relative to *Rnase1*$^{+/+}$ mice. Furthermore, apparent FXI activity was increased more than 1000-fold in *Rnase1*$^{-/-}$ mice when coagulation was induced with a low (0.1 µM) concentration of soluble tissue factor. FIX activity was similar in the two genotypes (Fig. 6A).

The variations in FXII and FXI activity, depending on the method of inducing coagulation, cannot be explained by differences in plasma concentrations of FXII and FXI antigen in the two mouse lines. Indeed, antigen concentrations of these proteins were similar in *Rnase1*$^{-/-}$ and *Rnase1*$^{+/+}$ mice on an immunoblot (Fig. 6B,C).

Rnase1$^{-/-}$ mice do not exhibit coagulation abnormalities in vivo

Rnase1$^{-/-}$ mice did not exhibit significant differences from *Rnase1*$^{+/+}$ mice in bleeding models (Fig. 7A–E), indicating that elevated plasma RNA did not have a deleterious effect on normal blood coagulation in vivo (hemostasis). This finding is in keeping with the observations that FXII and FXI are not required for hemostasis in mice (Pauer et al. 2004; Wang et al. 2005). Thrombin–antithrombin (TAT) complex formation was not different in *Rnase1*$^{+/+}$ and *Rnase1*$^{-/-}$ mice after treatment with lipopolysaccharide (LPS). LPS treatment results in a significant up-regulation of tissue factor, leading to increased thrombin generation. FXII and FXI would not be expected to have a major impact on such a process. Finally, there were no differences in thrombus formation in $FeCl_3$-induced arterial thrombosis assays, and fixed sections of the carotid artery revealed a similar distribution of degrees of vessel occlusion in both genotypes.

DISCUSSION

From a biochemical and biophysical perspective, RNase A is perhaps the most thoroughly studied enzyme (D'Alessio and Riordan 1997; Raines 1998; Marshall et al. 2008; Cuchillo et al. 2011). Still, little is known about the function of this protein or its homologs in vivo. We report on the use of reverse genetics to create an *Rnase1*$^{-/-}$ mouse. These animals are viable and fertile, but have marked reductions in plasma ribonucleolytic activity, resulting in increased plasma RNA concentration that affects the behavior of the plasma proteases FXII and FXI. These findings support the conclusion that RNA in plasma is physiologically important, and that one of the functions of RNase 1 is to regulate plasma RNA concentration.

Preissner and coworkers have shown that infusing RNase A into mice reduced thrombosis induced by arterial injury and concluded that RNA is a natural procoagulant in blood (Kannemeier et al. 2007). Thrombus formation in the model they used requires the plasma protein FXII. FXII along with prekallikrein and the cofactor high molecular weight kininogen (HK) comprise the plasma kallikrein–kinin system (Schmaier 2005). FXII and PK can undergo reciprocal conversion to the active proteases FXIIa and kallikrein by a process (contact activation) that is enhanced by binding to various "surfaces" that often carry a net negative charge. Polyanions such as RNA, DNA, and polyphosphate have been implicated as inducers of contact activation in vivo (Schmaier 2005; Morrissey and Smith 2015).

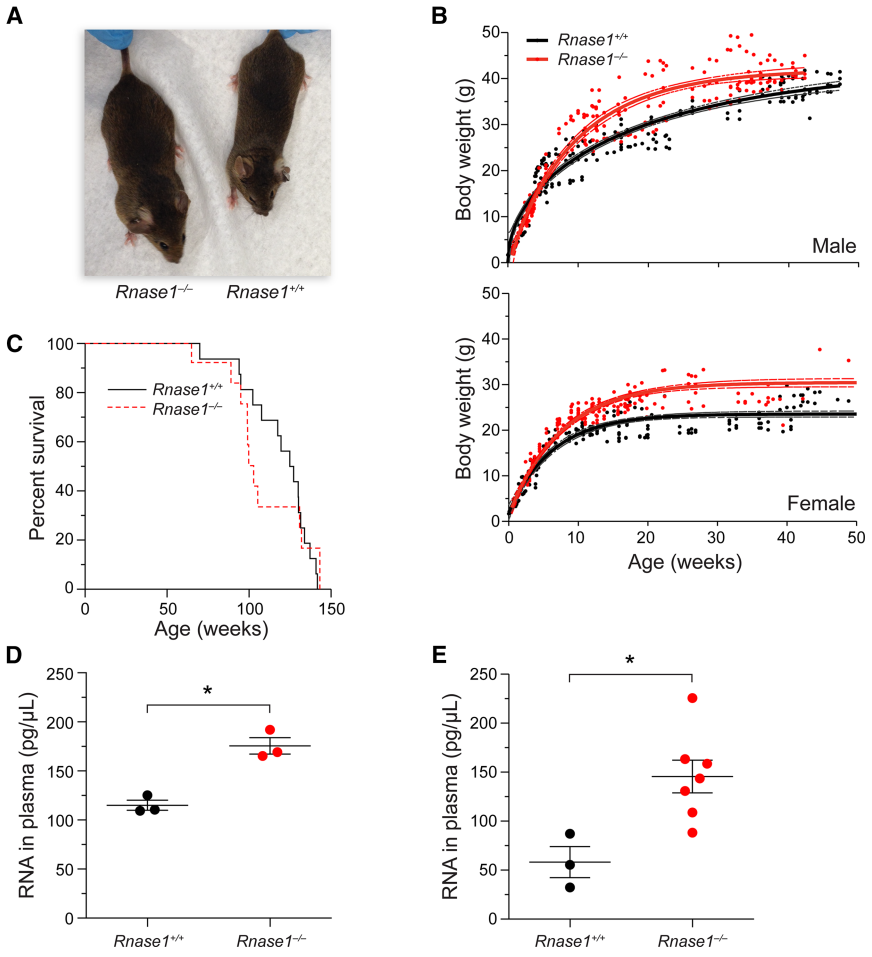

FIGURE 4. General phenotyping and longevity studies of *Rnase1*$^{-/-}$ mice. (*A*) Photograph of *Rnase1*$^{-/-}$ and *Rnase1*$^{+/+}$ mice that are 8-wk-old male littermates. (*B*) Graph showing the weekly weight of male *Rnase1*$^{-/-}$ and *Rnase1*$^{+/+}$ mice, $n \geq 5$. By 8 wk of age, male *Rnase1*$^{-/-}$ mice (29.7 ± 1 g) were significantly heavier than were male *Rnase1*$^{+/+}$ mice (22.8 ± 1 g); graph showing the weekly weight of female *Rnase1*$^{-/-}$ and *Rnase1*$^{+/+}$ mice, $n \geq 5$. By 8 wk of age, female *Rnase1*$^{-/-}$ mice (23.4 ± 0.5 g) were significantly heavier than were female *Rnase1*$^{+/+}$ mice (19.2 ± 0.4 g). (*C*) Graph showing the longevity of *Rnase1*$^{-/-}$ and *Rnase1*$^{+/+}$ mice, revealing no differences between survival by genotype. $n \geq 12$. (*D*) Graph showing the RNA content of *Rnase1*$^{-/-}$ and *Rnase1*$^{+/+}$ plasma as measured by spectrophotometry. Values are from purified RNA samples and are normalized to plasma volume. (*E*) Graph showing the RNA content of *Rnase1*$^{-/-}$ and *Rnase1*$^{+/+}$ plasma as measured with a Bioanalyzer electrophoresis system. Values are from purified RNA samples and are normalized to plasma volume. (*) $P < 0.05$.

that levels of the activated forms of at least some coagulation factors are increased in the plasma of *Rnase1*$^{-/-}$ mice. The observations that plasma clotting times wherein coagulation was induced with tissue factor were shorter for *Rnase1*$^{-/-}$ mice than for *Rnase1*$^{+/+}$ animals, whereas clotting times were similar in reactions with aPTT reagent, points to increased activity in the classic intrinsic pathway of coagulation in *Rnase1*$^{-/-}$ mice.

The intrinsic pathway is comprised of the components of the kallikrein–kinin system, and the plasma clotting proteins factors IX and VIII. The activity levels of factors XII, XI, and IX were measured with one-stage clotting assays, in which an unknown plasma is tested for its capacity to restore clotting in a reagent plasma lacking the protein of interest. Results are compared to those of a standard plasma assigned an activity value of 100%. Values in excess of 100% indicate that the concentration of a protein is higher than that of the control plasma. This conclusion is based on the assumption that the clotting factor being measured is in its inactive precursor form at the start of the assay. If this assumption is valid, then results for different types of assays should agree on the activity level, and the activity level and antigen level should match. When these equivalences are not observed, then the active forms of one or more clotting factors are likely present in plasma prior to the start of the assay. This latter circumstance was observed for FXII and FXI in *Rnase1*$^{-/-}$ mice.

FXIIa activity contributes to several host defense mechanisms, including inflammation through the generation of kallikrein and coagulation through the conversion of the plasma protein FXI to the serine protease FXIa. Although the latter reaction is not required for normal blood clot formation at a site of vessel injury (hemostasis), it is implicated in thrombosis and other pathologic processes (Maas and Renné 2018).

Our studies indicate that increased RNA in the plasma of *Rnase1*$^{-/-}$ mouse has effects on FXII and FXI. Specifically, RNA supports conversion of these proteins to their active forms. The shortened recalcification clotting times (clotting in the absence of aPTT reagent or tissue factor) indicate

There was an apparent 100-fold discrepancy in FXII activity as determined by recalcification times and aPTT assays in plasma from *Rnase1*$^{-/-}$ mice, consistent with the presence of significant amounts of FXIIa in the plasma before the initiation of coagulation. The observation that the apparent increase in FXII activity was not accounted for by an increase in FXII antigen supports this conclusion. RNA induces FXII autoactivation and enhances PK activation by FXIIa (Kannemeier et al. 2007; Ivanov et al. 2017). Although FXIIa in plasma might be expected to result in increased FXIa levels, that is not necessarily the case. In patients with deficiency of the FXIIa and kallikrein regulator C1 inhibitor, the consequence of unregulated FXIIa

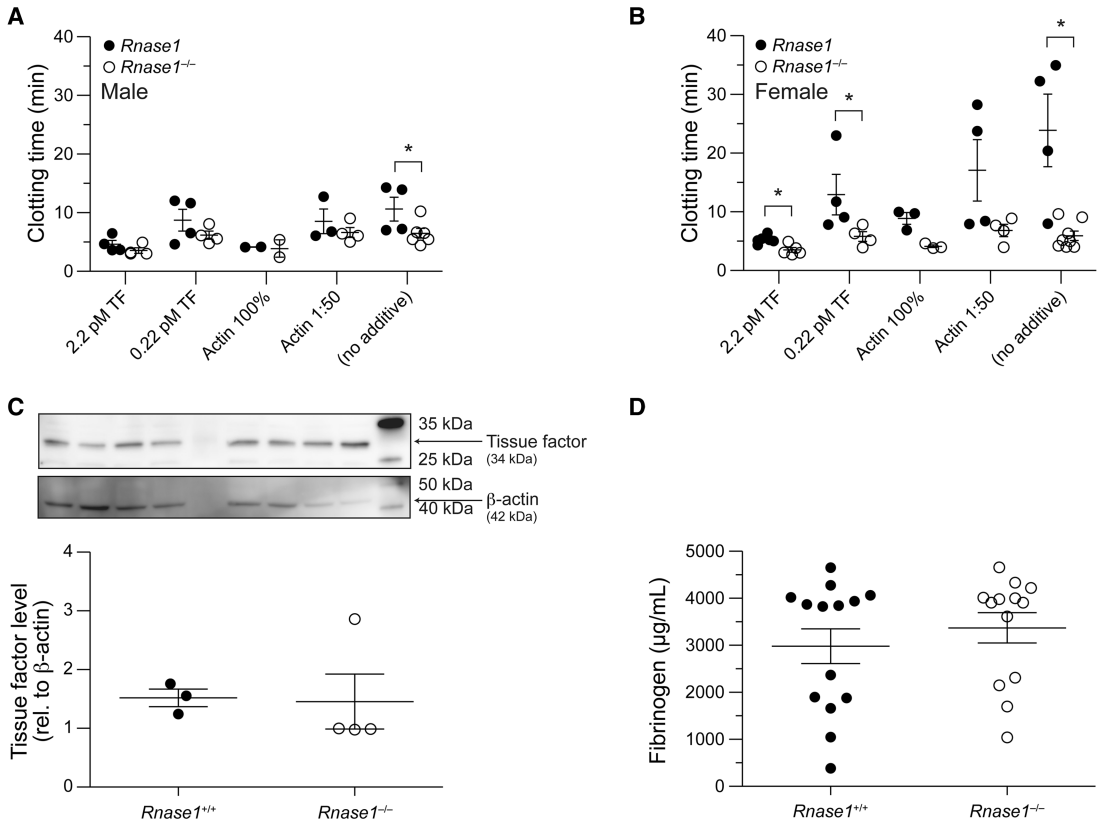

FIGURE 5. Effect of *Rnase1* on coagulation in vitro. (*A*) Graph showing the effect of activators Thromborel S (TF) and Actin FSL aPTT reagent (Actin) on the clotting of plasma from male mice. *Rnase1*$^{-/-}$ plasma from mice clots significantly faster than does *Rnase1*$^{+/+}$ plasma in the absence of added activator. $n \geq 3$. (*B*) Graph as in panel *A* but with female mice. *Rnase1*$^{-/-}$ plasma clots significantly faster than does *Rnase1*$^{+/+}$ plasma in the absence of added activator and in the presence of Thromborel S. $n \geq 3$. (*C*) Representative immunoblot to probe for tissue factor in the liver and graph showing the quantitation of band intensities in *Rnase1*$^{-/-}$ and *Rnase1*$^{+/+}$ mice. No significant difference was detected in the tissue factor level by genotype. $n = 4$. (*D*) Graph showing the fibrinogen level of plasma as assayed by ELISA in *Rnase1*$^{-/-}$ and *Rnase1*$^{+/+}$ mice. No significant difference was detected in fibrinogen level by genotype. $n = 13$. (*) $P < 0.05$.

activity is enhanced bradykinin generation and tissue swelling (angioedema), and not excessive coagulation (thrombosis). Increased FXIIa, then, does not necessarily translate into increased coagulation.

The results for FXI activity in this study are particularly intriguing. FXI levels based on recalcification times, aPTT assays, and coagulation induced with a saturating concentration of tissue factor roughly agreed with each other, and with results from *Rnase1*$^{+/+}$ mice, which indicated relatively little FXIa in plasma from *Rnase1*$^{-/-}$ mice. Nonetheless, assays using a low concentration of tissue factor indicated an ~10^3-fold higher level of FXI relative to plasma from *Rnase1*$^{+/+}$ mice. As with FXII, this increase was not accounted for by differences in the plasma FXI antigen levels. Polyanions, including RNA, enhance FXI activation by thrombin (Ivanov et al. 2017). This enhancement contributes little to clotting times in assays with saturating tissue factor because the initial burst of generated thrombin overwhelms contributions from the intrinsic pathway. At low tissue factor concentrations, however, the slower rate of thrombin generation allows feedback activation of FXI to FXIa by thrombin to affect the clotting time (Kravtsov et al. 2009). The large apparent increase in FXI activity, as determined by clotting in the presence of low tissue factor, is consistent with the presence of a polyanionic cofactor such as RNA in the plasma of *Rnase1*$^{-/-}$ mice.

It is important to note that elevated RNA levels in *Rnase1*$^{-/-}$ mice did not affect hemostatic or thrombotic responses appreciably in vivo. In the case of the hemostatic response to blood vessel injury, this result is not surprising, as a process that primarily affects FXII and FXI would not be expected to have much impact on hemostasis (Pauer et al. 2004). Although elevated plasma RNA levels in *Rnase1*$^{-/-}$ mice might have rendered the animals more prone to injury-induced thrombosis, local tissue damage could have masked the effects of plasma RNA. It does seem reasonable to conclude, however, that the elevated RNA in *Rnase1*$^{-/-}$ mice was not sufficient to induce thrombosis by itself. Still, our results indicate that elevated plasma RNA enhances the basal level of FXII activation, which

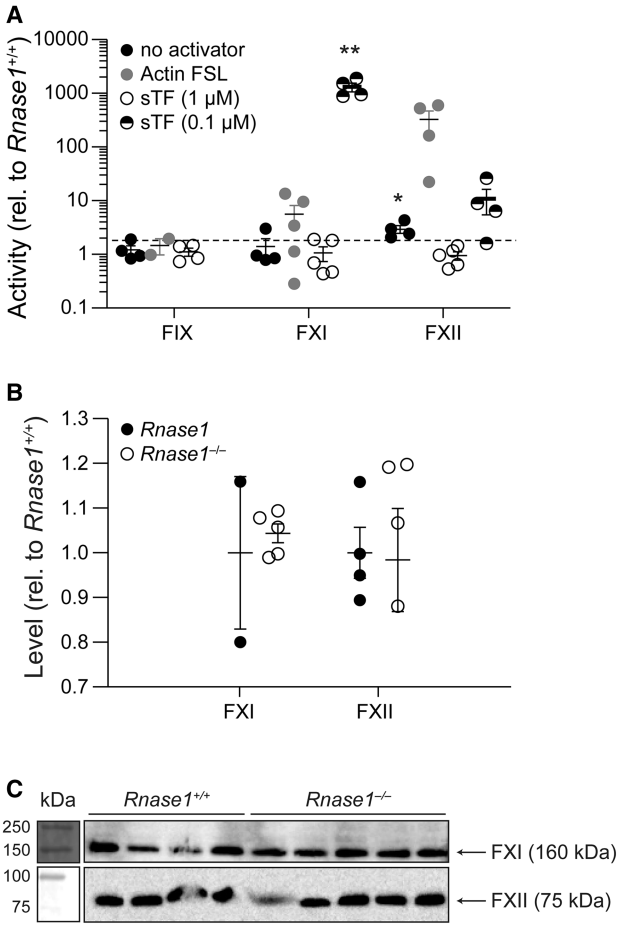

FIGURE 6. Effect of *Rnase1* on the levels of FXII and FXI. (*A*) Graph showing the activity of FIX, FXI, and FXII in the plasma of *Rnase1*$^{-/-}$ relative to that in *Rnase1*$^{+/+}$ mice. $n \geq 3$. (*B*) Graph showing the level of FXI and FXII in the plasma of *Rnase1*$^{-/-}$ and *Rnase1*$^{+/+}$ mice, normalized to the average expression in *Rnase1*$^{+/+}$ mice. $n \geq 3$. (*C*) Representative immunoblots to probe for FXI and FXII. Molecular weight markers are indicated from separate exposures. (*) $P < 0.05$; (**) $P < 0.001$.

might predispose animals to inflammation or thrombosis in the context of injury, infection, or cancer (Leon et al. 1977; Garcia et al. 2008; Fischer et al. 2013).

Differences in coagulation in vitro appear to be more robust by genotype in female mice than in male mice. This distinction could be due to hormonal differences between sexes, as hormonal contraceptive use and pregnancy are known to influence risk for aberrant blood clot formation (Artero et al. 2012; Bleker et al. 2014). Indeed, the FXII gene in humans is known to contain an estrogen-response element (Farsetti et al. 1995). Our analyses used nulliparous mice, but were performed in sexually mature mice and did not control for the estrus cycle in females, which could have contributed to trends in the data.

RNase 1 is one of ~25 homologous ptRNases in mice (Cho et al. 2005). The mild phenotype resulting from the loss of RNase 1 could be due to functional redundancy, with RNase 1 homologs performing crucial RNA-regulatory functions (Cormier et al. 2001; Dyer and Rosenberg 2005). The importance of such functions is suggested by the increase in activity of other ptRNases in *Rnase1*$^{-/-}$ mice, which could mitigate the consequences of RNase 1 loss. RNase 4, which is up-regulated in *Rnase1*$^{-/-}$ mice, is a likely candidate to compensate, as it exhibits similar substrate preferences and is also expressed broadly (Sorrentino 2010).

The cause of the increased body weight of *Rnase1*$^{-/-}$ mice was not established by our studies but is not explicable by differences in food or water consumption, or body fat. *Rnase1*$^{-/-}$ mice do, however, have slightly longer bodies than *Rnase1*$^{+/+}$ mice (data not shown). This difference suggests changes in growth factor activity in *Rnase1*$^{-/-}$ mice.

Given the proposed roles for RNA and RNase 1 in host defense, cancer, and blood coagulation (Sorrentino 2010; Koczera et al. 2016; Lu et al. 2018), our findings likely reveal only one of the biological functions of this enzyme, but do have implications for multiple processes. FXIIa promotes kallikrein formation, which in turn cleaves HK to liberate the vasoactive peptide bradykinin (Iwaki and Castellino 2006; Kaplan and Joseph 2014), an important mediator of inflammation and vascular permeability (Golias et al. 2007). Cancer patients are prone to coagulopathy (Falanga et al. 2014), and tumor-associated and circulating cancer cells express tissue factor (Falanga et al. 2015; Mitrugno et al. 2016) and activate FXII (Nickel et al. 2016). Moreover, RNA stimulates proinflammatory cytokine release, including tumor necrosis factor α (TNFα) and vascular endothelial growth factor (VEGF), promoting tumor cell growth and immune cell recruitment (Fischer et al. 2012, 2013). Plasma RNA could affect these biological processes, and a major function of RNase 1 could be to regulate such effects. We note, too, that eRNA secondary structure is thought to be important for its procoagulant activity (Gansler et al. 2012). Human RNase 1, which has higher activity against double-stranded RNA than does either mouse RNase 1 or RNase A (Eller et al. 2014; Lomax et al. 2017), might be better adapted to regulate endogenous eRNA alone.

MATERIALS AND METHODS

Materials

Murine ribonuclease 1 (RNase 1) and ribonuclease A were produced in *E. coli* as described previously (delCardayré et al. 1995; Lomax et al. 2014). PNGase F was from New England BioLabs. Human FXI-, FXII-, and PK-deficient plasma was from George King Bio-Medical. Murine FXI- and FXII-deficient plasma (Gailani et al. 1997; Pauer et al. 2004), and FIX-deficient plasma (Lin et al. 1997) were obtained as described. Soluble

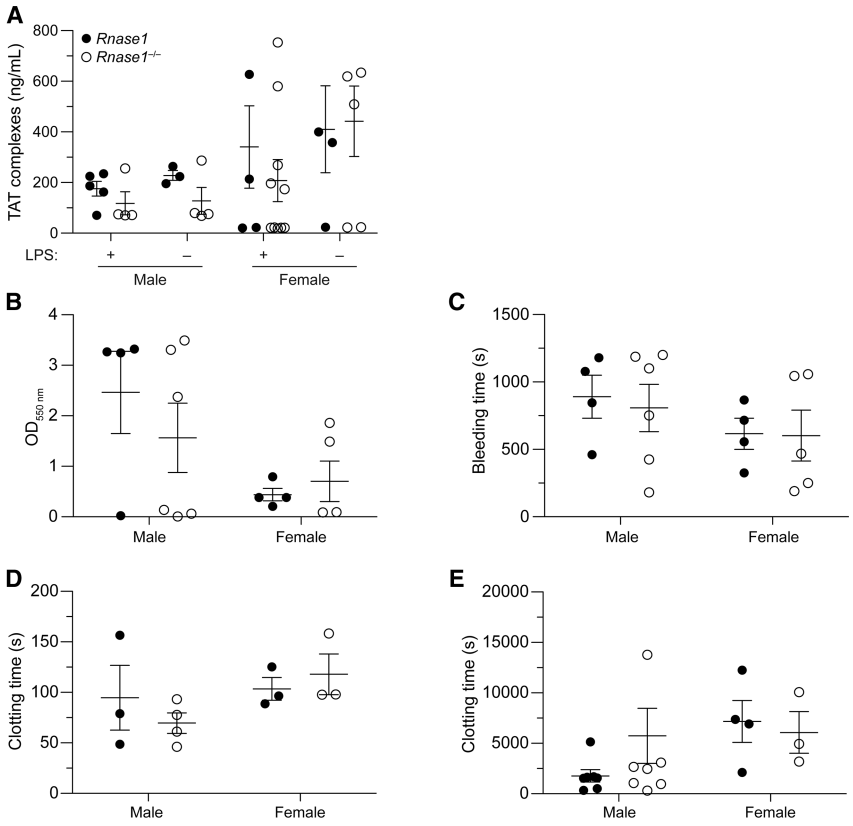

FIGURE 7. Effect of *Rnase1* on coagulation in vivo. (*A*) Graph showing the effect of LPS (2 mg/kg) on the level of TAT complex in the plasma of *Rnase1*$^{-/-}$ and *Rnase1*$^{+/+}$ mice. No significant difference was detected in complex level by genotype. $n \geq 3$. (*B*) Graph showing blood loss in tail-vein bleeding assays. No significant difference was detected in blood loss by genotype. $n \geq 4$. (*C*) Graph showing bleeding time in tail-vein bleeding assays. No significant difference was detected in bleed time by genotype. $n \geq 4$. (*D*) Graph showing clotting time in the carotid artery upon administration of ferric chloride. No significant difference was detected in clotting time by genotype. $n \geq 4$. (*E*) Graph showing clotting time in the saphenous vein. No significant difference was detected in clotting time by genotype. $n \geq 3$.

tissue factor was a gift from B.S. Schwartz (University of Wisconsin–Madison).

Phosphatidylserine (PS), phosphatidylcholine (PC), and cholesterol were from Avanti Polar Lipids. PC:PS:C (molar ratio, 75:25:20) phospholipid vesicles were prepared by extrusion through a 100-nm polycarbonate filter. Primers, DNA constructs, and the 6-FAM–dArUdAdA–6-TAMRA ribonuclease substrate were from Integrated DNA Technologies. Poly(cytidylic acid) and LPS were from Sigma–Aldrich.

Equipment

Fluorescence measurements were made with a Tecan M1000 fluorescence plate reader.

Conditions

All procedures were performed at ambient temperature (~22°C) and pressure (1.0 atm) unless noted otherwise.

Generation of *Rnase 1* knockout mice

All experiments with animals were conducted in accord with an Institution on Animal Care and Use Committee-approved protocol at the University of Wisconsin–Madison. Ribonuclease 1 KO mice (*Rnase1*$^{-/-}$) were generated by using recombineering methods (Liu et al. 2003). The *Rnase1* targeting vector was generated via homologous recombination in *E. coli*. To target the mouse *Rnase1* gene for deletion in vivo, loxP sites were engineered within intronic sequences to flank exon 2 (which contains the entire coding sequence of the gene), marking this region for eventual excision by Cre recombinase. A neomycin-resistance (*Neo*) cassette, flanked by FRT sequences, was inserted for positive selection, and thymidine kinase (TK) was included for negative selection. The targeting vector was introduced into 129Sv/Ev murine embryonic stem (ES) cells, and positively selected clones were verified with a Southern blot. Correctly targeted clones were sequenced to confirm that all loxP and FRT sites were present and intact. Male germline chimeras were mated to wild-type C57Bl/6 females, transmitting the targeted *Rnase1* allele. Karyotype analysis and chromosome counting was performed at the Molecular Cytogenetics Laboratory at Yale University. Blastocyst injection was performed by the University of Wisconsin–Madison Transgenic Animal Facility.

Ribonuclease 1-deficient mice (*Rnase1*$^{-/-}$) were generated with assistance from the University of Wisconsin–Madison Transgenic Animal Facility. The KO mice were produced in a C57BL6J (Stock 000664, Jackson Laboratories)/129SvJ (embryonic stem cells, Genome Systems) background. Neomycin-resistance cassettes used for selection were removed by crossing transgenic mice with FLP deleter mice (Stock 009086, Jackson Laboratories), and constitutive KO of *Rnase1* was achieved by crossing *Rnase1*$^{flox/flox}$ mice with ubiquitously driven CMV–Cre mice (Stock 009086, Jackson Laboratories) (Fig. 1B). The genotypic analysis of *Rnase1*$^{-/-}$ mice was performed by using a universal primer set for the *Rnase1* locus: forward 5′-TGCAGGGACTAGGGTAGTGG-3′ and reverse 5′-CATGACACAGGACAGGAACG-3′. This primer set produces a 797-bp band for the wild-type locus, a 2.77-kb band for the transgenic locus + neomycin-resistance cassette, a 2.08-kb band for the KO locus + neomycin-resistance cassette, a 973-bp band for the transgenic locus—neomycin-resistance cassette, and a 286-bp band for the KO locus—neomycin-resistance cassette (Fig. 1C,D). The phenotypic analysis of *Rnase1*$^{-/-}$ mice was carried out prior to the completion of backcrossing, and the experimental cohorts have a mixed C57Bl6/129SvJ background. To control for this mixed genetic background, all phenotypic analyses were

conducted with *Rnase1*$^{+/+}$ littermates of *Rnase1*$^{-/-}$ mice serving as age- and sex-matched controls.

Quantitative PCR

Quantitative real-time PCR (qPCR) was conducted to identify gene expression changes in *Rnase1*$^{-/-}$ mice. RNA was isolated from tissue samples homogenized in TRIzol Reagent (Invitrogen) using a Benchmark D1000 homogenizer, purified according to the manufacturer's protocol, DNase-treated using the TURBO DNA-free Kit (Thermo Fisher Scientific), and subjected to reverse transcription–PCR using the qScript cDNA Synthesis Kit (Quanta Biosciences). cDNA preparations were probed for *Rnase1*, *Rnase4*, *Ang1*, and *Rnh1* message using primer pairs shown in Table 1. Reactions were run in duplicate using SYBR Green master mix (Quanta Biosciences) with an Applied Biosystems ABI 7500 Fast Real-Time PCR system. Cycling conditions were 95°C for 30 sec, 55°C for 30 sec, and 72°C for 30 sec, repeated for 30 cycles and monitored by melting curves. Cycle threshold (C_T) values were determined by setting a constant threshold at 0.6; fold changes in gene expression were determined by the comparative C_T method (Schmittgen and Livak 2008). Expression was normalized to that of *Gapdh*, *Rpl13a*, and *Hprt1*.

Gross phenotypic analysis

The viability of *Rnase1*$^{-/-}$ mice was determined with a χ^2-squared test. Fertility was assessed by pairing *Rnase1*$^{-/-}$ male × *Rnase1*$^{+/+}$ female, *Rnase1*$^{+/+}$ male × *Rnase1*$^{-/-}$ female, and *Rnase1*$^{-/-}$ × *Rnase1*$^{-/-}$ mice for mating. In longevity studies, aged mice were killed upon exhibiting signs of illness or distress (e.g., significant weight loss, tumors, reduced movement, or responsiveness).

Gross physical analysis and histopathological analysis of mice were performed by the University of Wisconsin–Madison Research Animal Resource Center Comparative Pathology Laboratory.

Preparation of plasma samples

Whole blood was collected by cardiac puncture into citrate-rinsed syringes immediately prior to mixing with 3.2% w/v sodium citrate (citrate/blood 1:9). Blood was subjected to centrifugation at 2400*g* for 10 min at 4°C to prepare platelet-poor plasma for subsequent assays. Plasma samples were aliquoted and snap-frozen, then stored at −80°C until the time of analysis. For mixing tests, blood was drawn from the inferior vena cava and prepared similarly.

Ribonucleolytic activity assay

As a proxy for protein concentration, solution-phase assays of ribonucleolytic activity were performed on plasma samples, using a fluorogenic substrate described previously (Kelemen et al. 1999). The background fluorescence intensity (I_0) of 100 mM Tris–HCl buffer, pH 7.0, containing 6-FAM–dArUdAdA–6-TAMRA (10 µM), NaCl (100 mM), and acetylated bovine serum albumin (0.1 mg/mL) was measured. A 1-µL aliquot of plasma was added, and the change in fluorescence intensity (ΔI) over time was monitored with $\lambda_{ex} = 490$ nm and $\lambda_{em} = 525$ nm. Excess RNase A was added, and maximum fluorescence intensity (I_{max}) was measured. Recombinant murine RNase 1 was used to measure $k_{cat}/K_M = 8.6 \times 10^6$ M^{-1} sec^{-1}, which is indistinguishable from the value at pH 6.4 reported previously (Lomax et al. 2017). This value was, in turn, used to estimate the concentration of ribonuclease in mouse plasma with Equation 1:

$$[\text{ribonuclease}] = \frac{\Delta I}{\dfrac{I_{max} - I_0}{\dfrac{k_{cat}}{K_M}}}. \quad (1)$$

The ensuing value of [ribonuclease] is only an estimate because other plasma ribonucleases could differ in their k_{cat}/K_M values for the cleavage of 6-FAM–dArUdAdA–6-TAMRA.

Ribonuclease zymogram assay

Zymograms were performed on plasma samples to verify the loss of RNase 1 in *Rnase1*$^{-/-}$ mice, using an assay similar to one reported previously (Bravo et al. 1994). Briefly, a polyacrylamide gel containing SDS (0.1% w/v), Tris (375 mM), and poly(cytidylic acid) (4.5 mg, incubated at 50°C prior to addition) was cast. Samples containing recombinant murine RNase 1 (100 pmol) or murine plasma (0.5 µL) were prepared with 2× Laemmli sample buffer (without dithiothreitol or β-mercaptoethanol, and without boiling). Some samples were prepared from murine plasma pretreated by incubating 2 µL of plasma with 1000 U of PNGase F (New England BioLabs) for 48 h to remove *N*-linked glycans

TABLE 1. Primers used for qPCR

Target	Forward (5′ → 3′)	Reverse (3′ → 5′)
Rnase1	CTGCAAGAACAGGAAGAGCAAC	GAGTGGTCTTGTAGTCACAGTTGG
Rnase4	AACGGTTCCTTCGACAGCAT	GCGTTTGCACTGGACAGAAG
Ang1	TCTGCAGGGTTCAGACATGT	TCTGGGCTATGAGGGGAGAT
Rnh1	CCCAGCTGTAAGCTCAGGAC	CTCTGCTTGGCTCTGAGGAC
Gapdh	CTCCCACTCTTCCACCTTCG	CCACCACCCTGTTGCTGTAG
Rpl13a	GCTGAAGCCTACCAGAAAGT	TCCGTTTCTCCTCCAGAGT
Hprt1	CTAGTCCTGTGGCCATCTGC	GGGACGCAGCAACTGACATT

Gene IDs: *Rnase1*, 19752; *Rnase4*, 58809; *Ang1*, 11727; *Rnh1*, 107702; *Gapdh*, 14433; *Rpl13a*, 22121; *Hprt1*, 15452.

from RNase 1 (Ressler and Raines 2019). After electrophoresis, the gel was washed twice in 10 mM Tris–HCl buffer, pH 7.5, containing isopropanol (20% v/v), then once in 10 mM Tris–HCl buffer, pH 7.5, before incubation overnight in 100 mM Tris–HCl buffer, pH 7.5 to allow RNase 1 to refold within the gel. During the next day, the gel was washed in 10 mM Tris–HCl buffer, pH 7.5 before staining in an aqueous solution of toluidine (0.2% w/v) for 10 min. The gel was washed with deionized water and destained in 10 mM Tris–HCl buffer, pH 7.5. Band intensity was evaluated with ImageJ software (Schneider et al. 2012).

Quantitation of RNA in plasma

The size and amount of RNA in mouse plasma was evaluated independently by using either a NanoVue Plus Spectrophotometer (GE Healthcare) or a 2100 Bioanalyzer electrophoresis system and associated RNA kit (Agilent). RNA was isolated from plasma with the TRIzol Reagent and TURBO DNA-free Kit as described above. For spectrophotometery, RNA ($A_{260\ nm}/A_{280\ nm} \sim 2.0$) was quantified by absorbance using the Beer–Lambert law and $\varepsilon = 0.025\ mg^{-1} \cdot cm^{-1} \cdot mL$ at 260 nm. RNA concentrations were normalized to the volume of plasma.

Plasma coagulation assays

Coagulation assays were performed on mouse plasma using a variation on published procedures (Jagadeeswaran et al. 2000). Briefly, mixtures contained plasma (10 µL), human fibrinogen (100 µg; Sigma–Aldrich), and PC:PS:C vesicles (4 µM), were induced to clot with $CaCl_2$ (6 mM). The reaction volume was increased to 100 µL by adding 20 mM HEPES–HCl buffer, pH 7.35, containing NaCl (20 mM) and BSA (1% w/v). A variation of the prothrombin time (PT) assay was conducted by adding 5 µL of Thromborel S solution (Dade), diluted in the same buffer to final concentrations of 2.2 pM (high tissue factor) or 0.22 pM (limiting tissue factor). A variation of the aPTT time assay was conducted by adding 5 µL of Actin FSL Activated PTT reagent (Dade), at full strength or diluted 1:50. Clot formation was followed by monitoring $A_{405\ nm}$ over a period of ≤1 h. Clotting times are reported as the time at which the value of $A_{405\ nm}$ was half-maximal.

Coagulation factor activity assays

Activity assays for plasma factor IX, FXI, FXII, and prekallikrein were carried out by a mixing test using a variation of the kinetic coagulation assay described above. Briefly, 10 µL of factor-deficient human plasma was incubated with 10 µL of sample plasma to complement factor activity absent in the deficient plasma. (Sample was diluted in factor-deficient plasma in ratios ranging from 1:5 to 1:100, yielding samples with 20% to 1% of the normal factor activity.)

Some mixing tests were also performed with a Start 4 Hemostasis Analyzer (Diagnostica Stago). Briefly, 50 µL of factor-deficient human plasma was incubated with 25 µL of sample plasma (diluted in factor-deficient plasma) and 50 µL of Actin FSL Activated PTT reagent for 3 min at 37°C. An aqueous solution of $CaCl_2$ (17 mM) was added to initiate coagulation, and the time to clot formation was recorded.

Standard curves of factor activity as a function of plasma clotting time were generated by testing a pooled plasma set of five *Rnase1*$^{+/+}$ mice and plotting clotting time (y) against plasma dilution factor (expressed as percent activity of undiluted plasma) on a log-linear chart, and the y-intercept (b) and slope (m) were calculated. Factor activity in *Rnase1*$^{-/-}$ plasma relative to *Rnase1*$^{+/+}$ plasma was calculated with Equation 2:

$$\text{activity} = 10^{\frac{y-b}{m}}. \quad (2)$$

ELISA and immunoblotting

An ELISA was performed to evaluate plasma fibrinogen content. Assays were performed with a Mouse Fibrinogen ELISA Kit (Abcam) according to the manufacturer's instructions.

Relative plasma concentrations for FXI, FXII, PK, and high molecular weight kininogen (HK) were determined by nonreducing immunoblotting using chemiluminescence. FXI was detected with biotinylated anti-mouse FXI IgG 14E11 and streptavidin-HRP (Cheng et al. 2010). FXII and PK were detected with polyclonal goat antihuman FXII or anti-human PK IgG conjugated to HRP (Affinity Biologicals). HK was detected with polyclonal rabbit IgG raised against mHK1-specific sequence, and donkey anti-rabbit IgG-HRP (Merkulov et al. 2008). Blots were imaged using a c600 system (Azure Biosystem) and band strength was assessed with ImageJ software (Schneider et al. 2012).

The relative expression of tissue factor in liver was determined by immunoblotting. Briefly, tissue samples were homogenized with a Benchmark D1000 homogenizer in T-PER Tissue Protein Extraction Reagent (Thermo Fisher Scientific). Homogenized tissue and plasma samples were tested for protein content by using a bicinchoninic acid protein assay kit (Thermo Fisher Scientific) and prepared with denaturing sample buffer prior to SDS–PAGE. Samples were transferred to a membrane using the iBlot 2 Dry Blotting System (Thermo Fisher Scientific) for 1 min at 20 V, 2 min at 23 V, and 1 min at 25 V. Membranes were blocked for 1 h in 5% w/v dry milk in Tris-buffered saline with Tween (TBST, which contained 19 mM Tris base, 137 mM NaCl, 2.7 mM KCl, and 0.1% v/v Tween 20), and incubated overnight at 4°C with antibody. Tissue factor was detected with a rabbit polyclonal IgG (Bioss Antibodies), and β-actin with a rabbit monoclonal IgG (Cell Signaling Technology). The membrane was washed in TBST before a 1-h incubation at room temperature with a secondary antibody, diluted with an aqueous solution of dry milk (5% w/v) in TBST, then washed in TBST again before imaging. The blot was treated with SuperSignal West Pico Chemiluminescent substrate (Thermo Fisher Scientific) and imaged with an ImageQuant LAS 4000 imager (GE Healthcare), and band intensity was evaluated with ImageJ software (Schneider et al. 2012). Blots were stripped by using Restore Western Blot Stripping Buffer (Thermo Fisher Scientific) and probed again.

Thrombin–antithrombin complex formation assay

Thrombin–antithrombin (TAT) complex formation was measured as a marker of clot formation in response to LPS using a protocol adapted from one reported previously (Sommeijer et al. 2005). Briefly, mice were injected intraperitoneally with LPS (2 mg/kg

in sterile saline) or an equivalent volume of saline. After 4 h, mice were killed via exsanguination. Plasma was then assayed for TAT complex content by using a TAT Complexes Mouse ELISA Kit (Abcam) according to the manufacturer's instructions.

Tail-vein bleeding time assay

Tail-bleeding assays were performed as described previously (Liu et al. 2012). Briefly, mice were anesthetized with isoflurane and placed on a warming pad, and a 2-mm section of distal tail was amputated. Blood was collected into warm saline, and total bleeding time (including all rebleeding events) was recorded using a stopwatch. Collected blood cells were lysed, and the $A_{550\ nm}$ value of the lysate was used as a quantitative measure of blood loss.

Saphenous vein hemostasis assay

Hemostasis in the saphenous vein was assessed by using a protocol adapted from one reported previously (Buyue et al. 2008). Briefly, the left saphenous vein of an anesthetized mouse was dissected free of membranes and punctured with a 27 g needle. Time-to-cessation of bleeding was recorded, and the clot was dislodged by wiping the vein in the direction of blood flow to allow rebleeding. This procedure was repeated for 30 min while recording the number of clots and the average time to clot.

$FeCl_3$-induced thrombosis assay

Ferric-chloride induced arterial thrombosis assays were carried out with assistance from the University of Wisconsin–Madison Cardiovascular Physiology Core Laboratory. The left carotid artery of anesthetized mice was dissected and blotted before application of an aqueous solution of ferric chloride (10% w/v) using a 1 × 2 mm square of tissue. This solution was left in place for 3 min before washing the tissue with phosphate-buffered saline. After removal of the $FeCl_3$ solution, an ultrasound gel was applied and Doppler ultrasound was used to identify the carotid artery and measure blood flow rate for 30 min. A clot was judged to have formed when blood flow dropped to <10% of its initial rate. Mice were killed at the conclusion of the experiment, and carotid artery sections were collected into 4% neutral buffered formalin for fixation and staining.

Statistical analyses

A minimum of three biological replicates were performed for every experiment. All values are expressed as the mean ± SEM, and statistical evaluation was performed by Wilcoxon rank-sum test, log-rank test, and χ^2 test using Prism software (GraphPad) and MSTAT software (Michigan State University), with $P < 0.05$ being considered significant.

SUPPLEMENTAL MATERIAL

Supplemental material is available for this article.

ACKNOWLEDGMENTS

We are grateful to M.C. Haigis for initiating this project. We thank T.A. Hacker and the Cardiovascular Physiology Core at the University of Wisconsin–Madison for technical assistance with thrombosis assays, and R. Sullivan for surgical and dissection training. We also thank C. Feldman and K.E. Tippins for technical assistance with the maintenance of mouse colonies and sample preparation. This work was supported by grant R01 CA073808 (National Institutes of Health). E.R.G. was supported by Molecular and Cellular Pharmacology Training Grant T32 GM008688 (NIH) and by a William H. Peterson Fellowship in Biochemistry (Department of Biochemistry, University of Wisconsin–Madison). J.E.L. was supported by a National Science Foundation Graduate Research Fellowship.

Received January 19, 2019; accepted April 27, 2019.

REFERENCES

Artero A, Tarín JJ, Cano A. 2012. The adverse effects of estrogen and selective estrogen receptor modulators on hemostasis and thrombosis. *Semin Thromb Hemost* **38:** 797–807. doi:10.1055/s-0032-1328883

Barnard EA. 1969. Biological function of pancreatic ribonuclease. *Nature* **221:** 340–344. doi:10.1038/221340a0

Beintema JJ, Wietzes P, Weickmann JL, Glitz DG. 1984. The amino acid sequence of human pancreatic ribonuclease. *Anal Biochem* **136:** 48–64. doi:10.1016/0003-2697(84)90306-3

Bleker SM, Coppens M, Middeldorp S. 2014. Sex, thrombosis and inherited thrombophilia. *Blood Rev* **28:** 123–133. doi:10.1016/j.blre.2014.03.005

Bravo J, Fernández E, Ribó M, de Llorens R, Cuchillo CM. 1994. A versatile negative-staining ribonuclease zymogram. *Anal Biochem* **219:** 82–86. doi:10.1006/abio.1994.1234

Buyue Y, Whinna HC, Sheehan JP. 2008. The heparin-binding exosite of factor IXa is a critical regulator of plasma thrombin generation and venous thrombosis. *Blood* **112:** 3234–3241. doi:10.1182/blood-2008-01-136820

Cabrera-Fuentes HA, Niemann B, Grieshaber P, Wollbrueck M, Gehron J, Preissner KT, Böning A. 2015. RNase1 as a potential mediator of remote ischaemic preconditioning for cardioprotection. *Eur J Cardiothorac Surg* **48:** 732–737. doi:10.1093/ejcts/ezu519

Cheng Q, Tucker EI, Pine MS, Sisler I, Matafonov A, Sun MF, White-Adams TC, Smith SA, Hanson SR, McCarty OJ, et al. 2010. A role for factor XIIa-mediated factor XI activation in thrombus formation in vivo. *Blood* **116:** 3981–3989. doi:10.1182/blood-2010-02-270918

Cho S, Beintema JJ, Zhang J. 2005. The ribonuclease A superfamily of mammals and birds: identifying new members and tracing evolutionary histories. *Genomics* **85:** 208–220. doi:10.1016/j.ygeno.2004.10.008

Cormier SA, Larson KA, Yuan S, Mitchell TL, Lindenberger K, Carrigan P, Lee NA, Lee JJ. 2001. Mouse eosinophil-associated ribonucleases: a unique subfamily expressed during hematopoiesis. *Mamm Genome* **12:** 352–361. doi:10.1007/s003350020007

Cuchillo CM, Nogués MV, Raines RT. 2011. Bovine pancreatic ribonuclease: fifty years of the first enzymatic reaction mechanism. *Biochemistry* **50:** 7835–7841. doi:10.1021/bi201075b

Cuthbert BJ, Burley KH, Goulding CW. 2018. Introducing the new bacterial branch of the RNase A superfamily. *RNA Biol* **15:** 9–12. doi:10.1080/15476286.2017.1387710

D'Alessio G, Riordan JF. 1997. *Ribonucleases: structures and functions.* Academic Press, New York.

D'Avino C, Palmieri D, Braddom A, Zanesi N, James C, Cole S, Salvatore F, Croce CM, De Lorenzo C. 2016. A novel fully human anti-NCL immunoRNase for triple-negative breast cancer therapy. *Oncotarget* **7:** 87016–87030. doi:10.18632/oncotarget.13522

delCardayré SB, Ribó M, Yokel EM, Quirk DJ, Rutter WJ, Raines RT. 1995. Engineering ribonuclease A: production, purification, and characterization of wild-type enzyme and mutants at Gln11. *Protein Eng* **8:** 261–273. doi:10.1093/protein/8.3.261

Dyer KD, Rosenberg HF. 2005. The mouse *RNase 4* and *RNase 5/ang 1* locus utilizes dual promoters for tissue-specific expression. *Nucleic Acids Res* **33:** 1077–1086. doi:10.1093/nar/gki250

Eller CH, Lomax JE, Raines RT. 2014. Bovine brain ribonuclease is the functional homolog of human ribonuclease 1. *J Biol Chem* **289:** 25996–26006. doi:10.1074/jbc.M114.566166

Falanga A, Russo L, Milesi V. 2014. The coagulopathy of cancer. *Curr Opin Hematol* **21:** 423–429. doi:10.1097/MOH.0000000000000072

Falanga A, Marchetti M, Russo L. 2015. The mechanisms of cancer-associated thrombosis. *Thromb Res* **135:** S8–S11. doi:10.1016/S0049-3848(15)50432-5

Farsetti A, Misiti S, Citarella F, Felici A, Andreoli M, Fantoni A, Sacchi A, Pontecorvi A. 1995. Molecular basis of estrogen regulation of Hageman factor XII gene expression. *Endocrinology* **136:** 5076–5083. doi:10.1210/endo.136.11.7588244

Fischer S, Nishio M, Dadkhahi S, Gansler J, Saffarzadeh M, Shibamiyama A, Kral N, Baal N, Koyama T, Deindl E. 2011. Expression and localisation of vascular ribonucleases in endothelial cells. *Thromb Haemost* **105:** 345–355. doi:10.1160/TH10-06-0345

Fischer S, Grantzow T, Pagel JI, Tschernatsch M, Sperandio M, Preissner KT, Deindl E. 2012. Extracellular RNA promotes leukocyte recruitment in the vascular system by mobilising proinflammatory cytokines. *Thromb Haemost* **108:** 730–741. doi:10.1160/TH12-03-0186

Fischer S, Gesierich S, Griemert B, Schanzer A, Acker T, Augustin HG, Olsson AK, Preissner KT. 2013. Extracellular RNA liberates tumor necrosis factor-α to promote tumor cell trafficking and progression. *Cancer Res* **73:** 5080–5089. doi:10.1158/0008-5472.CAN-12-4657

Futami J, Tsushima Y, Murato Y, Tada H, Sasaki J, Seno M, Yamada H. 1997. Tissue-specific expression of pancreatic-type RNases and RNase inhibitor in humans. *DNA Cell Biol* **16:** 413–419. doi:10.1089/dna.1997.16.413

Gailani D, Lasky NM, Broze GJ Jr. 1997. A murine model of factor XI deficiency. *Blood Coagul Fibrinolysis* **8:** 134–144. doi:10.1097/00001721-199703000-00008

Gajsiewicz JM, Smith SA, Morrissey JH. 2017. Polyphosphate and RNA differentially modulate the contact pathway of blood clotting. *J Biol Chem* **292:** 1808–1814. doi:10.1074/jbc.M116.754325

Gansler J, Jaax M, Leiting S, Appel B, Greinacher A, Fischer S, Preissner KT. 2012. Structural requirements for the procoagulant activity of nucleic acids. *PLoS One* **7:** e50399. doi:10.1371/journal.pone.0050399

Garcia JM, Garcia V, Pena C, Dominguez G, Silva J, Diaz R, Espinosa P, Citores MJ, Collado M, Bonilla F. 2008. Extracellular plasma RNA from colon cancer patients is confined in a vesicle-like structure and is mRNA-enriched. *RNA* **14:** 1424–1432. doi:10.1261/rna.755908

Golias C, Charalabopoulos A, Stagikas D, Charalabopoulos K, Batistatou A. 2007. The kinin system-bradykinin: biological effects and clinical implications. Multiple role of the kinin system-bradykinin. *Hippokratia* **11:** 124–128.

Hoang TT, Tanrikulu IC, Vatland QA, Hoang TM, Raines RT. 2018. A human ribonuclease variant and ERK-pathway inhibitors exhibit highly synergistic toxicity for cancer cells. *Mol Cancer Ther* **17:** 2622–2632. doi:10.1158/1535-7163.MCT-18-0724

Ivanov I, Shakhawat RB, Sun MF, Dickeson SK, Puy C, McCart OJT, Gruber A, Matafonov A, Gailani D. 2017. Nucleic acids as cofactors for Factor XI and prekallikrein activation: different roles for high-molecular-weight kininogen. *Thromb Haemost* **117:** 671–681. doi:10.1160/TH16-09-0691

Iwaki T, Castellino FJ. 2006. Plasma levels of bradykinin are suppressed in factor XII-deficient mice. *Thromb Haemost* **95:** 1003–1110. doi:10.1160/TH06-03-0128

Jagadeeswaran P, Gregory M, Johnson S, Thankavel B. 2000. Haemostatic screening and identification of zebrafish mutants with coagulation pathway defects: an approach to identifying novel haemostatic genes in man. *Br J Haematol* **110:** 946–956. doi:10.1046/j.1365-2141.2000.02284.x

Kannemeier C, Shibamiya A, Nakazawa F, Trusheim H, Ruppert C, Markart P, Song Y, Tzima E, Kennerknecht E, Niepmann M, et al. 2007. Extracellular RNA constitutes a natural procoagulant cofactor in blood coagulation. *Proc Natl Acad Sci* **104:** 6388–6393. doi:10.1073/pnas.0608647104

Kaplan AP, Joseph K. 2014. Pathogenic mechanisms of bradykinin mediated diseases: dysregulation of an innate inflammatory pathway. *Adv Immunol* **121:** 41–89. doi:10.1016/B978-0-12-800100-4.00002-7

Kelemen BR, Klink TA, Behlke MA, Eubanks SR, Leland PA, Raines RT. 1999. Hypersensitive substrate for ribonucleases. *Nucleic Acids Res* **27:** 3696–3701. doi:10.1093/nar/27.18.3696

Koczera P, Martin L, Marx G, Schuerholz T. 2016. The ribonuclease A superfamily in humans: canonical RNases as the buttress of innate immunity. *Int J Mol Sci* **17:** 1278. doi:10.3390/ijms17081278

Kravtsov DV, Matafonov A, Tucker EI, Sun M-F, Walsh PN, Gruber A, Gailani D. 2009. Factor XI contributes to thrombin generation in the absence of factor XII. *Blood* **114:** 452–458. doi:10.1182/blood-2009-02-203604

Landré JB, Hewett PW, Olivot JM, Friedl P, Ko Y, Sachinidis A, Moenner M. 2002. Human endothelial cells selectively express large amounts of pancreatic-type ribonuclease (RNase 1). *J Cell Biochem* **86:** 540–552. doi:10.1002/jcb.10234

Leon SA, Shapiro B, Sklaroff DM, Yaros MJ. 1977. Free DNA in the serum of cancer patients and the effect of therapy. *Cancer Res* **37:** 646–650.

Lin H-F, Maeda N, Smithies O, Straight DL, Stafford DW. 1997. A coagulation factor IX-deficient mouse model for human hemophilia B. *Blood* **90:** 3962–3966.

Liu P, Jenkins NA, Copeland NG. 2003. A highly efficient recombineering-based method for generating conditional knockout mutations. *Genome Res* **13:** 476–484. doi:10.1101/gr.749203

Liu Y, Jennings NL, Dart AM, Du XJ. 2012. Standardizing a simpler, more sensitive and accurate tail bleeding assay in mice. *World J Exp Med* **2:** 30–36. doi:10.5493/wjem.v2.i2.30

Lomax JE, Bianchetti CM, Chang A, Phillips GN Jr, Fox BG, Raines RT. 2014. Functional evolution of ribonuclease inhibitor: insights from birds and reptiles. *J Mol Biol* **426:** 3041–3056. doi:10.1016/j.jmb.2014.06.007

Lomax JE, Eller CH, Raines RT. 2017. Comparative functional analysis of ribonuclease 1 homologs: molecular insights into evolving vertebrate physiology. *Biochem J* **474:** 2219–2233. doi:10.1042/BCJ20170173

Lu L, Li J, Moussaoui M, Boix E. 2018. Immune modulation by human secreted RNases at the extracellular space. *Front Immunol* **9:** 1012. doi:10.3389/fimmu.2018.01012

Maas C, Renné T. 2018. Coagulation factor XII in thrombosis and inflammation. *Blood* **131:** 1903–1909. doi:10.1182/blood-2017-04-569111

Marshall GR, Feng JA, Kuster DJ. 2008. Back to the future: ribonuclease A. *Biopolymers* **90:** 259–277. doi:10.1002/bip.20845

Merkulov S, Zhang WM, Komar AA, Schmaier AH, Barnes E, Zhou Y, Lu X, Iwaki T, Castellino FJ, Luo G, et al. 2008. Deletion of murine kininogen gene 1 (*mKng1*) causes loss of plasma kininogen and delays thrombosis. *Blood* **111:** 1274–1281. doi:10.1182/blood-2007-06-092338

Mitrugno A, Tormoen GW, Kuhn P, McCarty OJ. 2016. The prothrombotic activity of cancer cells in the circulation. *Blood Rev* **30:** 11–19. doi:10.1016/j.blre.2015.07.001

Morita T, Niwata Y, Ohgi K, Ogawa M, Irie M. 1986. Distribution of two urinary ribonuclease-like enzymes in human organs and body fluids. *J Biochem (Tokyo)* **99:** 17–25. doi:10.1093/oxfordjournals.jbchem.a135456

Morrissey JH, Smith SA. 2015. Polyphosphate as modulator of hemostasis, thrombosis, and inflammation. *J Thromb Haemost* **13 (Suppl 1):** S92–S97. doi:10.1111/jth.12896

Nickel KF, Labberton L, Long AT, Langer F, Fuchs TA, Stavrou EX, Butler LM, Renné T. 2016. The polyphosphate/factor XII pathway in cancer-associated thrombosis: novel perspectives for safe anticoagulation in patients with malignancies. *Thromb Res* **141:** S4–S7. doi:10.1016/S0049-3848(16)30353-X

Pauer H-U, Renné T, Hemmerlein B, Legler T, Fritzlar S, Adham I, Müller-Esterl W, Emons G, Sancken U, Engel W. 2004. Targeted deletion of murine coagulation factor XII gene—a model for contact phase activation *in vivo*. *Thromb Haemost* **92:** 503–508. doi:10.1160/TH04-04-0250

Raines RT. 1998. Ribonuclease A. *Chem Rev* **98:** 1045–1066. doi:10.1021/cr960427h

Ressler VT, Raines RT. 2019. Consequences of the endogenous *N*-glycosylation of ribonuclease 1. *Biochemistry* **58:** 987–996. doi:10.1021/acs.biochem.8b01246

Salazar VA, Rubin J, Moussaoui M, Pulido D, Nogués MV, Venge P, Boix E. 2014. Protein post-translational modification in host defense: the antimicrobial mechanism of action of human eosinophil cationic protein native forms.. *FEBS J* **281:** 5432–5446. doi:10.1111/febs.13082

Samad F, Ruf W. 2013. Inflammation, obesity, and thrombosis. *Blood* **122:** 3415–3422. doi:10.1182/blood-2013-05-427708

Schmaier AH. 2005. The contact activation and kallikrein/kinin systems: pathophysiologic and physiologic activities. *J Thromb Haemost* **14:** 28–39. doi:10.1111/jth.13194

Schmittgen TD, Livak KJ. 2008. Analyzing real-time PCR data by the comparative C_T method. *Nat Protoc* **3:** 1101–1108. doi:10.1038/nprot.2008.73

Schneider CA, Rasband WS, Eliceiri KW. 2012. NIH Image to ImageJ: 25 years of image analysis. *Nat Methods* **9:** 671–675. doi:10.1038/nmeth.2089

Simsekyilmaz S, Cabrera-Fuentes HA, Meiler S, Kostin S, Baumer Y, Liehn EA, Weber C, Boisvert WA, Preissner KT, Zernecke A. 2014. Role of extracellular RNA in atherosclerotic plaque formation in mice. *Circulation* **129:** 598–606. doi:10.1161/CIRCULATIONAHA.113.002562

Sommeijer DW, van oerle R, Reitsma PH, Timmerman JJ, Meijers JC, Spronk HM, ten Cate H. 2005. Analysis of blood coagulation in mice: pre-analytical conditions and evaluation of a home-made assay for thrombin–antithrombin complexes. *Thromb J* **3:** 12. doi:10.1186/1477-9560-3-12

Sorrentino S. 2010. The eight human "canonical" ribonucleases: molecular diversity, catalytic properties, and special biological actions of the enzyme proteins. *FEBS Lett* **584:** 2194–2200. doi:10.1016/j.febslet.2010.04.018

Strong LE, Kink JA, Mei B, Shahan MN, Raines RT. 2012. First-in-human phase I clinical trial of QBI-139, a human ribonuclease variant, in solid tumors. *J Clin Oncol* **30:** TPS3113. doi:10.1158/1535-7163.targ-09-c42

Su AI, Wiltshire T, Batalov S, Lapp H, Ching KA, Block D, Zhang J, Soden R, Hayakawa M, Kreiman G, et al. 2004. A gene atlas of the mouse and human protein-encoding transcriptomes. *Proc Natl Acad Sci* **101:** 6062–6067. doi:10.1073/pnas.0400782101

Walberer M, Tschernatsch M, Fischer S, Ritschel N, Volk K, Friedrich C, Bachmann G, Mueller C, Kaps M, Nedelmann M, et al. 2009. RNase therapy assessed by magnetic resonance imaging reduces cerebral edema and infarction size in acute stroke. *Curr Neurovasc Res* **6:** 12–19. doi:10.2174/156720209787466037

Wang X, Cheng Q, Xu L, Feuerstein GZ, Hsu M-Y, Smith PL, Seiffert DA, Schumacher WA, Ogletree ML, Gailani D. 2005. Effects of factor IX or factor XI deficiency on ferric chloride-induced carotid artery occlusion in mice. *J Thromb Haemost* **3:** 695–702. doi:10.1111/j.1538-7836.2005.01236.x

Weickmann JL, Olson EM, Glitz DG. 1984. Immunological assay of pancreatic ribonuclease in serum as an indicator of pancreatic cancer. *Cancer Res* **44:** 1682–1687. doi:10.1016/b978-0-08-030764-0.50134-8